Published in final edited form as:
*J Neurochem*. 2008 August ; 106(4): 1563–1576. doi:10.1111/j.1471-4159.2008.05501.x.

# ER $Ca^{2+}$ dysregulation and ER stress following *in vitro* neuronal ischemia: role of $Na^{+}$-$K^{+}$-$Cl^{-}$ cotransporter

**Xinzhi Chen**[1,2], **Douglas B. Kintner**[2], **Jing Luo**[2,3], **Akemichi Baba**[4], **Toshio Matsuda**[4], and **Dandan Sun**[1,2,3]

[1]Neuroscience Training Program, Univ. of Wisconsin School of Medicine and Public Health, Madison, WI 53792

[2]Dept. of Neurological Surgery, Univ. of Wisconsin School of Medicine and Public Health, Madison, WI 53792

[3]Dept. of Physiology, Univ. of Wisconsin School of Medicine and Public Health, Madison, WI 53792

[4]Graduate School of Pharmaceutical Sciences, Osaka University, Osaka, Japan

## Abstract

We investigated the role of $Na^{+}$-$K^{+}$-$Cl^{-}$ cotransporter (NKCC1) in conjunction with $Na^{+}/Ca^{2+}$ exchanger (NCX) in disruption of endoplasmic reticulum (ER) $Ca^{2+}$ homeostasis and ER stress development in primary cortical neurons following *in vitro* ischemia. Oxygen-glucose deprivation (OGD) and reoxygenation (REOX) caused a rise in $[Na^{+}]_{cyt}$ which was accompanied by an elevation in $[Ca^{2+}]_{cyt}$. Inhibition of NKCC1 with its potent inhibitor bumetanide abolished the OGD/REOX-induced rise in $[Na^{+}]_{cyt}$ and $[Ca^{2+}]_{cyt}$. Moreover, OGD significantly increased $Ca^{2+}{}_{ER}$ accumulation. Following REOX, a biphasic change in $Ca^{2+}{}_{ER}$ occurred with an initial release of $Ca^{2+}{}_{ER}$ which was sensitive to inositol 1,4,5-trisphosphate receptor ($IP_3R$) inhibition and a subsequent refilling of $Ca^{2+}{}_{ER}$ stores. Inhibition of NKCC1 activity with its inhibitor or genetic ablation prevented the release of $Ca^{2+}{}_{ER}$. A similar result was obtained with inhibition of reversed mode operation of NCX ($NCX_{rev}$). OGD/REOX also triggered a transient increase of glucose regulated protein 78 (GRP78), phospho-form of the alpha subunit of eukaryotic initiation factor 2 (p-eIF2α), and cleaved caspase 12 proteins. Pretreatment of neurons with NKCC1 inhibitor bumetanide inhibited upregulation of GRP78 and attenuated the level of cleaved caspase 12 and p-eIF2α. Inhibition of NKCC1 reduced cytochrome C release and neuronal death. Taken together, these results suggest that NKCC1 and $NCX_{rev}$ may be involved in ischemic cell damage in part via disrupting ER $Ca^{2+}$ homeostasis and ER function.

### Keywords

oxygen and glucose deprivation; ischemia-reperfusion; unfolded protein response; $IP_3$ receptor; caspase 12; eIF2α

**Address correspondence to:** Dandan Sun, M.D., Ph.D. Department of Neurological Surgery University of Wisconsin Medical School H4/332 Clinical Sciences Center 600 Highland Ave. Madison, WI 53792 Phone: (608) 263-4060, FAX: (608) 263-1409 sun@neurosurg.wisc.edu.

*We would like to thank Dr. Donald J. DeGracia for many helpful discussions and reading the manuscript. This work was supported in part by NIH grants R01NS38118 and R01NS048216 (D. Sun), and an AHA Established-Investigator award grant N0540154 (D. Sun).

## INTRODUCTION

Endoplasmic reticulum (ER) stress has received increased attention in ischemic neurodegeneration because it triggers the unfolded protein response (UPR). The UPR involves protein synthesis inhibition, activation of stress gene expression, and ER-associated protein degradation (DeGracia and Montie 2004; DeGracia and Hu 2007). There is direct evidence of ER stress following brain ischemia/reperfusion (DeGracia and Hu 2007; Hayashi et al. 2003; Hayashi et al. 2005). However, it is not well understood how the UPR is triggered following ischemia. Disruption of ER $Ca^{2+}$ ($Ca^{2+}_{ER}$) homeostasis plays an important role in induction of ER stress (Corbett and Michalak 2000; Groenendyk and Michalak 2005). Depletion of $Ca^{2+}_{ER}$ and ATP can disrupt proper peptide folding and trigger the UPR and ER stress. Numerous reports demonstrate that depletion of $Ca^{2+}_{ER}$ with the sarco/endoplasmic reticulum $Ca^{2+}$-ATPase (SERCA) inhibitor thapsigargin triggers ER stress and the UPR in many cell types (Groenendyk and Michalak 2005). Moreover, augmenting $Ca^{2+}_{ER}$ levels by overexpression of the ER $Ca^{2+}$ binding protein calreticulin or SERCA increases the amount of ER $Ca^{2+}$ available for release and amplifies mitochondrial cytochrome C (Cyt. C) release and apoptosis (Groenendyk and Michalak 2005). However, the cellular mechanisms underlying $Ca^{2+}_{ER}$ dysregulation and UPR effector activation following ischemia and reperfusion are not defined.

We hypothesize that dysregulation of $Ca^{2+}_{ER}$ homeostasis following ischemia involves two phases: accumulation of $Ca^{2+}$ in ER stores and subsequent release of $Ca^{2+}_{ER}$ following ischemia/reoxygenation (REOX). Both accumulation of $Ca^{2+}$ in ER stores and subsequent release of $Ca^{2+}_{ER}$ may contribute to ER stress and ischemic cell death. $Na^+$-$K^+$-$Cl^-$ cotransporter isoform 1 (NKCC1) transports $Na^+$, $K^+$, and $Cl^-$ in cells under physiological conditions (Russell 2000). Our previous studies demonstrated that NKCC1 in conjunction with $NCX_{rev}$ are important in disruption of $Na^+$ and $Ca^{2+}$ homeostasis following ischemia (Kintner et al. 2007; Lenart et al. 2004). However, it is unknown whether these transporter proteins indirectly contribute to changes of $Ca^{2+}_{ER}$ homeostasis and ER dysfunction following ischemia.

In the current study, we present first line evidence that NKCC1 and $NCX_{rev}$ are involved in $Ca^{2+}_{ER}$ dysregulation, which includes overload of $Ca^{2+}_{ER}$ during oxygen and glucose deprivation (OGD) and release of $Ca^{2+}_{ER}$ during REOX. $Ca^{2+}_{ER}$ dysregulation was accompanied with development of ER stress.

## MATERIALS AND METHODS

### Materials

Eagle's minimal essential medium (EMEM) and Hanks balanced salt solution (HBSS) were from Mediatech Cellgro (Herndon, VA). Fetal bovine serum (FBS) was from Valley Biomedical Inc. (Winchester, VA) and horse serum (HS) was from Hyclone Laboratories (Logan, UT). 1-[6-Amino-2-(5-carboxy-2-oxazolyl)-5-benzofuranyloxy]-2-(2-amino-5-methylphenoxy) ethane-N,N,N′,N′-tetraacetic acid (fura-2 AM), sodium-binding benzofuran isophthalate (SBFI-AM), furaptra-AM (mag-fura-2-AM), calcein-AM, 4-bromo A-23187 and Alexa Fluor 488 anti-mouse IgG were from Invitrogen (Carlsbad, CA). Pluronic acid was purchased from BASF (Ludwigshafen, Germany). Bumetanide, gramicidin, monensin, propidium iodide (PI), thapsigargin, xestospongin C, and (−)-MK-801 were purchased from Sigma (St. Louis, MO). 2-aminoethoxydiphenyl borate (2-APB) and 1-aminoindan-1, 5-dicarboxylic acid (AIDA) were from Tocris (Ellisville, MO). SEA0400 was a kind gift from Taisho Pharmaceutical CO. Ltd. (Omiya, Saitama, Japan). 4′, 6-diamidino-2-phenylindole (DAPI) was from Vector Laboratories (Burlingame, CA). Antibody for β tubulin type-III was from Promega (Madison, WI). Anti-GRP78 antibody was from Assay Design (Ann Arbor,

MI). Anti-caspase 12 antibody, anti-phospho-eIF2alpha (p-eIF2α) antibody, and anti-eIF2alpha (eIF2α) antibody were from Cell Signaling Technology (Danvers, MA). Anti-Cyt. C antibody was from Pharmingen (clone 6H2.B4, San Jose, CA).

## Enriched cortical neuron cultures

Wild-type ($NKCC1^{+/+}$) E14-16 pregnant mice (SV129/Black swiss) were anesthetized with 5% halothane and euthanized as described before (Beck et al. 2003). Fetuses were removed and the cortices were dissected in ice-cold HBSS (Beck et al. 2003). The tissues were treated with 0.5 mg/ml trypsin at 37°C for 25 min. The cells were centrifuged at 350 g for 4 min. The cell suspension was diluted in complete EMEM containing 5% FBS and 5% HS. The cells were seeded in 24-well plates or on glass coverslips coated with poly-D-lysine (800 cells/$mm^2$) and incubated at 37°C in an incubator with 5% $CO_2$ and atmospheric air. After 96 h, cultures were treated with 4 μM cytosine-β-D arabinofuranoside for 3 days. Cultures were re-fed with fresh medium every 3 days. Cultures at 10-15 days *in vitro* (DIV) were used in the study. This cortical neuron culture preparation contained 5–10% astrocytes.

In the experiments using cortical neurons cultured from NKCC1 homozygous mutant ($NKCC1^{-/-}$) mice, male and female gene-targeted NKCC1 heterozygous mutant ($NKCC1^{+/-}$) mice were bred as described before (Flagella et al. 1999). $NKCC1^{+/+}$ and $NKCC1^{-/-}$ cultures were established from the E14–16 fetuses (Chen et al. 2005). The genotype of each mouse was determined by a polymerase chain reaction of DNA from fetus tail biopsies (Su et al. 2002). Experiments were performed in parallel with the wild-type and knockout cells from the littermates.

## Oxygen and glucose deprivation (OGD) treatment

DIV 10-15 neuronal cultures were rinsed with an isotonic OGD solution (pH 7.4) containing (in mM): 0 glucose, 20 $NaHCO_3$, 120 NaCl, 5.36 KCl, 0.33 $Na_2HPO_4$, 0.44 $KH_2PO_4$, 1.27 $CaCl_2$, 0.81 $MgSO_4$, as described before (Lenart et al. 2004). This solution has a $K^+$ concentration (~ 5.8 mM) which is similar to the EMEM (5.4 mM) used for cell cultures. The cells were incubated in 1 ml of OGD solution for 2 h in a hypoxic incubator (model 3130, Thermo Forma, Marietta, OH) containing 94% $N_2$, 1% $O_2$, and 5% $CO_2$. The oxygen level in the OGD solution decreased to ~2-3% after 60 min in the hypoxic incubator (Beck et al. 2003). Normoxic control cells were incubated for 2 h in 5% $CO_2$ and atmospheric air in a buffer identical to the OGD solution except for the addition of 5.5 mM glucose. Reoxygenation (REOX) was achieved by addition of equal volume of EMEM with the final glucose concentration of 5.5 mM, and incubation at 37°C in 5% $CO_2$ and atmospheric air. The oxygen level was ~ 18% during reoxygenation on the stage.

## Intracellular $Na^+$ measurement

Intracellular $Na^+$ concentration ($[Na^+]_{cyt}$) was measured with the fluorescent dye SBFI-AM as described previously (Kintner et al. 2004). Cultured neurons grown on coverslips were loaded with 10 μM SBFI-AM plus 0.02% pluronic acid during 2 h OGD. In our previous study (Luo et al. 2005), 2 h OGD did not significantly decrease retention of calcein-AM fluorescence signal and fluorescent intensity of either pH indicator BCECF-AM, $Na^+$ dye SBFI-AM, or $Ca^{2+}$ dye fura-2-AM. Therefore, SBFI-AM or fura-2-AM was loaded during OGD throughout this study.

The coverslips were quickly (< 2 min) placed in an open-bath imaging chamber (Model RC24, Warner Instruments, Hamden, CT) and superfused (1 ml/min) with $HCO_3^-$-MEM at 37°C. $HCO_3^-$-MEM contained (in mM): 5.5 glucose, 20 $NaHCO_3$, 120 NaCl, 5.4 KCl, 0.33 $Na_2HPO_4$, 0.44 $KH_2PO_4$, 1.27 $CaCl_2$, 0.81 $MgSO_4$ and equilibrated with 5% $CO_2$, 21 % $O_2$, and 74 % $N_2$. Using a Nikon TE 300 inverted epifluorescence microscope and a 40X lens,

neurons were excited every 10 min at 345 nm and 385 nm and the emission fluorescence at 510 nm recorded. Images were collected and the 345/385 ratios analyzed with the MetaFluor image-processing software as described previously (Su et al. 2002). At the end of each experiment, absolute $[Na^+]_{cyt}$ was determined for each cell by performing an in-situ calibration as described before (Su et al. 2002).

### Intracellular $Ca^{2+}$ measurement

Neurons grown on coverslips were incubated with 5 μM fura-2 AM during 2 h OGD. This extended period of dye loading did not lead to compartmentalization of the dye into ER and mitochondria because permeablization of neurons with saponin (3 μg/ml for 30 sec) led to an approximately 94% loss of the fura-2 fluorescence from the cell, indicating little fura-2 was loaded in cellular organelles. Following OGD, the cells were quickly (< 2 min) placed in the open-bath imaging chamber and superfused with $HCO_3^-$-MEM at 37°C as described above. Using the Nikon TE 300 inverted epifluorescence microscope and a 40X objective lens, neurons were excited at either every 10 sec or every 5 min at 345 and 385 nm and the emission fluorescence at 510 nm recorded. Images were collected and analyzed with the MetaFluor image-processing software. At the end of each experiment, the cells were exposed to 1 mM $MnCl_2$ in $Ca^{2+}$-free $HCO_3^-$-MEM and 5 μM 4-bromo A-23187. The $Ca^{2+}$-insensitive fluorescence was subtracted (Luo et al. 2005) and the $MnCl_2$-corrected 345/385 emission ratios were converted to concentration using the Grynkiewicz equation (Grynkiewicz et al. 1985) as described previously (Lenart et al. 2004). A $K_d$ of 370 nM for fura-2 was used (Petr and Wurster 1997). $R_{min}$ was obtained in the presence of $Ca^{2+}$-free HEPES-MEM containing 10 mM EGTA and 5 μM 4-bromo A-23187. $R_{max}$ was from the ratio in HEPES-MEM containing 10 mM $Ca^{2+}$ and 5 μM 4-bromo A-23187 as well as 4 μM rotenone and 2 μM FCCP (to inhibit active mitochondrial $Ca^{2+}$ transport). The ionic composition of HEPES-MEM was similar to $HCO_3^-$-MEM except that 20 mM $NaHCO_3$ was replaced with 20 mM HEPES and NaCl adjusted to maintain constant $Na^+$ (Su et al. 2002).

### Determination of $NCX_{rex}$

$NCX_{rex}$ was determined in cultured neurons using the method of Urbanczyk et al. (Urbanczyk et al. 2006), which minimizes the confounding effects of $Ca^{2+}$ buffering by intracellular organelles. Briefly, cells on coverslips were loaded with 5 μM fura2-AM during either 2 h normoxia or OGD. Cells were then placed in HEPES-MEM and $[Ca^{2+}]_{cyt}$ was monitored as described above. After a 30 sec baseline, ER $Ca^{2+}$ stores were emptied by applying ATP (100 μM) and thapsigargin (1 μM) in a $Ca^{2+}$-free HEPES-MEM buffer. When a new baseline was established, a $Na^+$-free/low $Ca^{2+}$ (100 μM) HEPES buffer was applied to initiate $NCX_{rev}$. In the $Na^+$ free buffer, NaCl was replaced with equimolar levels of N-methyl-D-glutamine. $NCX_{rev}$ was quantified by fitting a slope to the increase in $[Ca^{2+}]_{cyt}$ over the first 30 sec.

### $Ca^{2+}_{ER}$ measurement

Neurons on coverslips were incubated with 4 μM mag-fura-2 AM and 0.02 % pluronic acid during 2 h OGD. Upon to REOX, the coverslip was quickly (< 2 min) placed on an open-bath imaging chamber in HEPES-MEM at 37°C. Cells were excited every 10 sec at 345 and 385 nm and the emission fluorescence images collected at 510 nm using Nikon TE 300 inverted epifluorescence microscope and a 40X objective lens. To determine $Ca^{2+}_{ER}$, first, the plasma membrane was permeablized with 30 sec exposure to saponin (3.0 μg/ml) in an intracellular solution to eliminate the cytosolic mag-fura-2 signal. Composition of the intracellular solution was (mM): 25 NaCl, 125 KCl, 10 HEPES, 3 $Na_2ATP$, 0.55 $CaCl_2$, and 1.0 EGTA with free $Ca^{2+}$ of ~150 nmol/ml using the Max chelator program (Tsien and Pozzan 1989). This treatment caused a decrease in cytosolic mag-fura-2 fluorescence (~ 60%, Figure 2C, a) but an increase in the ratio of 345nm/385nm ($F_{345/385}$, $R_{base}$), which reflects mag-fura-2 in ER. Next, $R_{min}$

was obtained with a minimum $F_{345/385}$ ratio in a $Ca^{2+}$-free solution (in mM, 25 NaCl, 125 KCl, 10 HEPES, 4 EGTA, 0.005 4-bromo A-23187, Figure 2C, c). $R_{max}$ was the maximum $F_{345/385}$ ratio in a high $Ca^{2+}$ solution (containing 10 mM $CaCl_2$, Figure 2C, d). The $Ca^{2+}{}_{ER}$ values were then calculated using the equation $\lfloor Ca^{2+}_{ER} \rfloor = K \times (R_{base} - R_{min}) / (R_{max} - R_{base})$. K was determined as 56 μM in neurons using solutions of known $Ca^{2+}$ concentrations (Calcium Calibration Buffer Kit, Invitrogen, Carlsbad, CA).

## Gel electrophoresis and Western blotting

Cells were washed with ice-cold PBS and lysed with 30 sec sonication at 4°C in anti-phosphatase buffer (pH 7.4) containing (mM): 145 NaCl, 1.8 $NaH_2PO_4$, 8.6 $Na_2HPO_4$, 100 NaF, 10 $Na_4P_2O_7$, 2 $Na_3VO_4$, 2 EDTA and 0.2 μM microcystin and protease inhibitors as described previously (Luo et al. 2005). Protein content was determined by the bicinchoninic acid method. Protein samples (60-80 μg/lane) and pre-stained molecular mass markers (Bio-Rad, Hercules, CA) were denatured in SDS 2X sample buffer and then electrophoretically separated on 8 or 10% SDS gels. The resolved proteins were electrophoretically transferred to a PVDF membrane (Kintner et al. 2004). The blots were incubated in 7.5% nonfat dry milk in tris-buffered saline (TBS) overnight at 4°C and then incubated for 1 h with a primary antibody. The blots were rinsed with TBS and incubated with horseradish peroxidase-conjugated secondary IgG for 1 h. Bound antibody was visualized using an enhanced chemiluminescence assay (Amersham Corp, Piscataway, NJ). Relative changes in protein expression were estimated from the mean pixel density of each protein band using the Scion Image program (Orem, Utah). Rabbit anti-GRP78 polyclonal antibody (1:1000), anti-caspase 12 polyclonal antibody (1:1000), anti-phosphorylated eIF2α (p-eIF2α) polyclonal antibody (1:500), or anti-eIF2α antibody (1:1000), and anti-β tubulin III monoclonal antibody (1:4000) were used.

## Cyt. C immunofluorescence

Cyt. C release was determined with a specific antibody staining against Cyt. C. Briefly, cells on coverslips were fixed in 4% paraformaldehyde in PBS for 10 min. After rinsing, cells were incubated with the blocking solution for 20 min followed by incubation at room temperature with the anti-Cyt. C antibody (1:100) for 1 h. After rinsing in PBS, coverslips were incubated with green-fluorescent Alexa Fluor 488 anti-mouse IgG (1:100) for 1 h at 37°C. The coverslips were then covered with Vectashield mounting medium with DAPI. Fluorescence images were captured by the Nikon TE 300 inverted epifluorescence microscope (60X) using a Princeton Instruments MicroMax CCD camera and MetaMorph image-processing software (Universal Imaging Corp., Downingtown, PA).

## Quantification of Cyt. C release from mitochondria

Cyt. C release into the cytosol was assessed in subcellular fraction preparations as described before. After removing the culture medium from the plates, cells were incubated in 2 ml of trypsin (0.2 mg/ml)-EDTA (1 mM) solution at 37°C for 10 min. The cells were detached and a cell suspension was prepared in 4 ml of EMEM. The cytosolic and mitochondrial fractions were isolated as described before and protein content in each fraction was determined (Luo et al. 2005). Levels of Cyt. C in cytosol and mitochondrial fractions were measured using the Quantikine M Rat/Mouse Cytochrome C Immunoassay kit (R&D Systems, Minneapolis, MN). Data were expressed as ng/mg protein.

## Measurement of cell death

Cell viability was assessed by PI uptake and retention of calcein using a Nikon TE 300 inverted epifluorescence microscope. Cultured neurons were rinsed with HEPES-MEM and incubated with 1 μM calcein-AM and 10 μg/ml PI in the same buffer at 37°C for 30 min. For cell counting, cells were rinsed with the isotonic control buffer and visualized using a Nikon 20X objective

lens. Calcein and PI fluorescences were visualized using FITC filters and Texas Red filters as described before (Beck et al. 2003). Images were collected using a Princeton Instruments MicroMax CCD camera. In a blind manner, a total of 1000 cells/condition were counted using MetaMorph image-processing software. Cell mortality was expressed as the ratio of PI-positive cells to the sum of calcein-positive and PI-positive cells.

### Measurement of $IP_3$ content

Following OGD/REOX, pure neuron cultures grown on coverslips were deproteinized in ice-cold OGD buffer containing 4% perchloric acid. The cell lystates were centrifuged (2000 g) and the resulting supernatant was neutralized with 1.5 M KOH in 60 mM HEPES. After centrifugation (2000 g), $IP_3$ content in an 100 μL aliquot of the supernatant was analyzed with the D-myo-inositol 1,4,5-triphosphate biotrak assay kit from Amersham (Piscataway, NJ). The radioactivity in each sample was determined in a liquid scintillation counter. Protein content was measured in sister coverslips subjected to identical treatments. Data were expressed as pmol/mg protein.

### Statistics

Statistical significance was determined by student's *t*-test or an ANOVA (Bonferroni post-hoc test) in the case of multiple comparisons. A *P*-value smaller than 0.05 was considered statistically significant. N values represent the number of cultures used in each experiment.

## RESULTS

### Changes in $[Na^+]_{cyt}$ and $[Ca^{2+}]_{cyt}$ are partially dependent on NKCC1 activity following OGD/REOX

A small increase in $[Na^+]_{cyt}$ occurred during 60 min of normoxic perfusion on the microscope stage (Figure 1 A). Two hours of OGD did not cause a significant increase in $[Na^+]_{cyt}$ as compared to normoxic neurons (15.5 ± 1.1 vs. 11.5 ± 0.9 mM Figure 1 A). In contrast, REOX triggered a progressive rise in $[Na^+]_{cyt}$ which reached 42.7 ± 6.1 mM after 60 min ($p < 0.05$). When NKCC1 was inhibited with 5 μM bumetanide, the increase in $[Na^+]_{cyt}$ at 60 min REOX was significantly reduced (29.1 ± 0.6 mM, $p < 0.05$).

$[Na^+]_i$ levels measured in this study are the net result of a balance between $Na^+$ efflux mediated by $Na^+$-$K^+$-ATPase and $Na^+$ influx mediated by various influx pathways, including NKCC1. To illustrate the real $Na^+$ rise, an experiment with 1 mM ouabain was performed. As shown in Figure 1 B, the rise of $[Na^+]_i$ was 13.8 $Na^+$ mM/min under normoxic conditions when $Na^+$-$K^+$-ATPase function was inhibited. The rate was not significantly changed (13.9 $Na^+$ mM/min ) during the first 30 min REOX after 2 h OGD. However, over 40 min these cells died and the SBFI dye leaked out of cells due to the $Na^+$ overload. This did not occur in normoxic control cells (Figure 1 C).

Sustained increases in $[Na^+]_{cyt}$ activate $NCX_{rev}$ and lead to an increase in $[Ca^{2+}]_{cyt}$ in astrocytes (Kintner et al. 2007). Thus, we monitored changes in $[Ca^{2+}]_{cyt}$ at 2 h OGD and during 0-60 min REOX (Figure 1 D). 2 h OGD led to a ~ 2-fold increase in $[Ca^{2+}]_{cyt}$ as compared to normoxic controls (140 ± 17 nM vs. 68 ± 5 nM). REOX triggered a significant secondary rise in $[Ca^{2+}]_{cyt}$ at 30 min and reached 334 ± 12 nM at 60 min REOX (Figure 1 D, $p < 0.05$). Inhibition of NKCC1 with 5 μM bumetanide during OGD did not affect the OGD-induced increase in $[Ca^{2+}]_{cyt}$, but abolished the secondary rise in $[Ca^{2+}]_{cyt}$ during 30-60 min REOX (187 ± 11 nM, $p < 0.05$). $[Ca^{2+}]_{cyt}$ returned to basal level when NMDA receptors and NKCC1 were blocked during 0-60 min REOX with NMDA receptor antagonist (−)-MK-801 and bumetanide, respectively (Figure 1 D). These data suggest that the initial rise in $[Ca^{2+}]_{cyt}$ is largely due to activation of NMDA receptors.

### Changes in $Ca^{2+}_{ER}$ following OGD/REOX in neurons

We then investigated whether $Ca^{2+}_{ER}$ was affected by OGD/REOX. First, we examined whether the OGD-induced rise in $[Ca^{2+}]_{cyt}$ would result in an accumulation of $Ca^{2+}$ in $Ca^{2+}_{ER}$ stores. 1 μM thapsigargin, an inhibitor of SERCA, was applied to neurons in the absence of extracellular $Ca^{2+}$ to measure releasable $Ca^{2+}$ from the $Ca^{2+}_{ER}$ stores (Figure 2 A, B). Thapsigargin triggered a transient increase in $[Ca^{2+}]_{cyt}$ that was resolved within 1-2 min (Figure 2 A). The integrated area ($IA_{Ca2+}$) under the $Ca^{2+}$ rise curve was 181 ± 41 nM×min. Following 2 h OGD, thapsigargin-induced changes in $IA_{Ca2+}$ were significantly increased (344 ± 39 nM×min, $p < 0.05$, Figure 2 A, B). When NKCC1 was inhibited with 5 μM bumetanide, the thapsigargin-induced release of $Ca^{2+}$ was markedly attenuated and not significantly different from normoxic controls. This suggests that OGD causes a significant $Ca^{2+}$ loading in $Ca^{2+}_{ER}$ stores and that involves NKCC1.

To further study kinetic changes in $Ca^{2+}_{ER}$, we directly measured $Ca^{2+}_{ER}$ in neurons using the low-affinity $Ca^{2+}$ dye mag-fura 2. The restriction of the mag-fura-2 signal to ER was confirmed by several experiments. First, as seen in Figure 2C, $F_{345/385}$ for mag-fura 2 increased when the plasma membrane was permeablized with 30 sec exposure to saponin (**top trace, a, b**) thereby eliminating the cytosolic mag-fura-2 signal. Secondly, removal of ATP from the intracellular solution caused an abrupt decrease in $F_{345/385}$, demonstrating that retention of $Ca^{2+}_{ER}$ via SERCA depends on ATP (Figure 2C, lower trace). Moreover, application of FCCP to the permeablized cells caused a small increase in $F_{345/385}$, presumably reflecting $Ca^{2+}$ taken up by ER after the FCCP-triggered mitochondrial $Ca^{2+}$ release (Figure 2D, top trace). In contrast, application of 1 μM thapsigargin resulted in an 85% loss in $F_{345/385}$ (Figure 2D, lower trace). Subsequent application of FCCP did not cause an increase in the $F_{345/385}$ because thapsigargin irreversibly inhibits SERCA. Taken together, these data strongly suggest that the $F_{345/385}$ signal is primarily from ER.

Basal level of $Ca^{2+}_{ER}$ in normoxic neurons was 8.6 ± 1.0 μM (Figure 2 E, F). Following 2 h OGD, $Ca^{2+}_{ER}$ increased by ~ 2.5-fold (21.9 ± 2.1 μM, $p < 0.05$, Figure 2 E, F), which is consistent with the findings of the thapsigargin experiments described above. Interestingly, there were transient changes in $Ca^{2+}_{ER}$ during 0-60 min REOX. 85% of the $Ca^{2+}_{ER}$ in ischemic neurons was released at 15 REOX (3.1 ± 0.9 μM, Figure 2 F). $Ca^{2+}_{ER}$ levels recovered at 30 min REOX and reached 9.5 ± 3.0 μM at 60 min REOX. In contrast, when 5 μM bumetanide was applied at the beginning of REOX, REOX failed to trigger the release of $Ca^{2+}_{ER}$ (Figure 2 F). $Ca^{2+}_{ER}$ remained overloaded at 15 min REOX (21.8 ± 2.4 μM). Only a small amount of $Ca^{2+}_{ER}$ was slowly released during 30-60 min REOX (~ 16.2 μM). However, delayed application of 5 μM bumetanide (at 15 min REOX) failed to block the release of $Ca^{2+}_{ER}$ and did not affect the subsequent refilling of $Ca^{2+}_{ER}$ stores (Figure 2 F). In addition, inhibition of $NCX_{rev}$ with the NCX reverse-mode inhibitor SEA0400 (1 μM) during 15 min REOX also blocked the OGD/REOX-induced $Ca^{2+}_{ER}$ release (Figure 2 F). Incubation of 5 μM bumetanide in normoxic neurons for 30 min did not significantly changed basal levels of $Ca^{2+}_{ER}$ (11.3 ± 2.1 μM, $n = 3$, $p > 0.05$).

Bumetanide inhibits NKCC1, $K^+$- $Cl^-$ cotransporters, and other anion transport processes (e.g., $Cl^-/HCO3^-$ exchange, $Cl^-$ channels etc.) at higher concentrations. Although the concentration of bumetanide (5 or 10 μM) used in this study is relatively specific for NKCC1 (Russell 2000), the role of NKCC1 in changes of $Ca^{2+}_{ER}$ was further confirmed in $NKCC1^{-/-}$ neurons. In contrast to an increase in $Ca^{2+}_{ER}$ in $NKCC1^{+/+}$ neurons at 2 h OGD (21.9 ± 2.1 μM), $NKCC1^{-/-}$ neurons exhibited significantly less $Ca^{2+}_{ER}$ accumulation (16.4 ± 0.8 μM, $n = 4$, $p < 0.05$). At 15 min REOX, no significant release of $Ca^{2+}_{ER}$ was detected in $NKCC1^{-/-}$ neurons (13.0 ± 2.2 μM, $n = 4$, $p > 0.05$). Taken together, these data suggest that OGD/REOX transiently perturbs $Ca^{2+}_{ER}$ homeostasis. NKCC1 activity not only contributes to $Ca^{2+}_{ER}$ overload during OGD, but also to the subsequent $Ca^{2+}_{ER}$ release. This further supports the view that activation

of NKCC1/$NCX_{rev}$ is involved in the $Ca^{2+}_{ER}$ accumulation and subsequent release of $Ca^{2+}_{ER}$.

### Inhibition of $IP_3$ receptors prevents OGD/REOX-mediated $Ca^{2+}_{ER}$ release

Release of $Ca^{2+}_{ER}$ following REOX could be mediated through several pathways including activation of $IP_3$ receptors ($IP_3R$). To investigate this possibility, we first determined if $IP_3$ levels in neurons were elevated during early REOX. Basal level of $IP_3$ in pure neuronal cultures averaged 0.32 ± 0.01 pmol/mg protein, but increased dramatically at 5 min REOX (12.8 ± 1.4 pmol/mg protein (Figure 3 A). $IP_3$ levels were further increased to 18.7 ± 1.7 pmol/mg protein at 10 min REOX. In the presence of 5 μM bumetanide, the OGD/REOX-mediated increase in $IP_3$ was decreased by ~ 50% at 5 min REOX (6.6 ± 1.04 pmol/mg protein). $IP_3$ remained significantly reduced at 10 min REOX when NKCC1 was inhibited by bumetanide (Figure 3 A).

We then investigated whether inhibition of the $IP_3R$ could affect $Ca^{2+}_{ER}$ release after OGD/REOX. When $IP_3R$ were inhibited during 0-15 min REOX with 2-APB, REOX-induced release of $Ca^{2+}_{ER}$ was blocked (~ 18.5 μM, Figure 3 B). To further establish the role of $IP_3R$ in REOX-mediated $Ca^{2+}_{ER}$ release, xestospongin C, a more potent inhibitor of $IP_3R$, was used. Xestospongin C (20 μM) applied during 0-15 min REOX completely prevented the REOX-mediated release of $Ca^{2+}_{ER}$ (~ 22.0 μM, Figure 3 B).

$IP_3$ production can be stimulated via activation of group I metabotropic glutamate receptors (mGluR I) and subsequent stimulation of phospholipase C (PLC). We further investigated the role of mGluR I in REOX-mediated $Ca^{2+}_{ER}$ release. Inhibition of mGluR I with the specific mGluR I antagonist AIDA (100 μM) during 0-15 min of REOX blocked ~ 66% of the REOX-induced release of $Ca^{2+}_{ER}$ (Figure 3 B). Taken together, the data suggest that $IP_3$ production and activation of $IP_3R$ lead to $Ca^{2+}_{ER}$ release following OGD/REOX.

### Inhibition of NKCC1 activity reduces OGD/REOX-induced ER stress in neurons

To elucidate the role of $Ca^{2+}_{ER}$ dysregulation in development of ER stress following OGD/REOX, expression of several ER stress markers was examined. Phosphorylation of eIF2α can be triggered by RNA-dependent protein kinase-like ER eIF2α kinase (PERK) activation following cerebral ischemia and reperfusion (Kumar et al. 2001; Paschen 2003). In the current study, the level of p-eIF2α did not change at 0 h REOX, but was dramatically increased at 0.25, 0.5, and 1 h REOX ($p < 0.05$, Figure 4 A). The peak level of p-eIF2α signal was ~ 4 fold of control at 0.25 h REOX. It remained elevated by ~ 2.5 fold at 1 h REOX and above the resting level at 24 h REOX (Figure 4 A). Interestingly, inhibition of NKCC1 with bumetanide during OGD and REOX (pretreatment) significantly attenuated OGD/REOX-mediated up-regulation of p-eIF2α ($p < 0.05$, Figure 4 B). Moreover, addition of bumetanide at 0 min REOX was effective in reducing p-eIF2α levels at 1 h REOX (Figure 4 C). Inhibition of NKCC1 starting at 15 min or 30 min REOX still had some protective effects. Consistent with the bumetanide result, $NKCC1^{-/-}$ neurons did not show up-regulation of p-eIF2α following OGD/REOX (Figure 4 B). Taken together, these results indicate that early REOX triggers ER stress and inhibition of NKCC1 activity reduces the level of p-eIF2α.

We also studied activation of caspase 12, a marker for ER stress-dependent apoptotic pathway (Glazner and Fernyhough 2002). Both procaspase 12 (60 kDa band) and the cleaved forms of caspase 12 (35 kDa and 50 kDa) were recognized by the anti-caspase12 antibody (Figure 5 A, B). The relative ratio of 35 plus 50 kDa /60 kDa intensity was calculated to reflect caspase 12 activation. 2 h OGD triggered caspase 12 activation by 80%. The level of cleaved caspase 12 remained elevated during 15-60 min REOX. It returned to control levels by 3 h REOX (Figure 5 A, B). Treatment of neurons with bumetanide during OGD and REOX significantly reduced

the activation of caspase 12 during 15-30 min REOX. Moreover, addition of bumetanide at 0, 15 or 30 min REOX was effective in reducing the activation of caspase 12 (Figure 5 C). Taken together, our results demonstrate that inhibition of NKCC1 not only attenuates the dysregulation of $Ca^{2+}_{ER}$ homeostasis during early REOX but also concurrently reduces caspase 12 cleavage following OGD/REOX.

GRP78 protein, a commonly used marker for ER stress, was up-regulated by ~ 50 % at 2 h OGD. This elevation continued at 3, 6, and 12 h REOX ($p < 0.05$, Figure 6 A, B). GRP78 protein level returned to baseline by 24 h REOX. Inhibition of NKCC1 activity during OGD and REOX blocked the up-regulation of GRP78 protein ($p < 0.05$, Figure 6 B).

## Prevention of $Ca^{2+}_{ER}$ dysregulation is neuroprotective

We further investigated whether prevention of $Ca^{2+}$ dysregulation reduces neuronal damage. First, we determined Cyt. C release. Normoxic control neurons express an abundant level of Cyt. C with a punctuate and perinuclear expression pattern (Figure 7 A a, green, arrow). Some punctate Cyt. C staining was also observed in neurites. DAPI staining shows normal nuclear morphology (Figure 7 A a, blue). In contrast, after 3 h OGD/1 h REOX, Cyt. C immunoreactive signals became diffuse in the cytosol in some neurons (Figure 7 A b, arrowhead). Moreover, some neurons lost Cyt. C immunoreactivity (*** in** Figure 7 A b). After 3 h OGD/21 h REOX, Cyt. C staining could not be detected in most neurons (Figure 7 A c). These neurons concurrently exhibited condensed or fragmented chromatin in the nuclei (*** in** Figure 7 A b & c). The loss of Cyt. C immunoreactive signals suggests that Cyt. C may be released from mitochondria and subsequently degraded following OGD/REOX. However, when NKCC1 activity was inhibited with 10 μM bumetanide, OGD/REOX-triggered Cyt. C release was significantly attenuated. Figure 7 A (**d**) illustrates strong Cyt. C immunoreactive signals in the bumetanide treated neurons with near normal nuclear morphology (Figure 7 A d, arrow).

To further quantify Cyt. C release, we measured Cyt. C content from cytosolic and mitochondrial fractions with an immunoassay. As shown in Figure 7 B, under control conditions, Cyt. C content in the cytosol was low (133 ± 21 ng/mg protein). OGD/REOX treatment led to a nearly ~ 2 fold increase in the cytosolic Cyt. C (289 ± 30 ng/mg protein). In contrast, mitochondrial Cyt.C was significantly decreased (399 ± 68 ng/mg protein, $p < 0.05$, Figure 7 B), compared to normoxic controls (944 ± 262 ng/mg protein). In the presence of bumetanide, Cyt. C release into cytosol was almost blocked (178 ± 22 ng/mg protein, $p < 0.05$). Consist with this, inhibition of NKCC1 activity with bumetanide prevented the decrease in the mitochondrial Cyt.C (854 ± 89 ng/mg protein, $p < 0.05$, Figure 7 B). Taken together, the data of immunostaining and immunoassay for Cyt. C consistently demonstrate that inhibition of NKCC1 activity preserves mitochondrial integrity in neurons following OGD/REOX.

We then examined the effects of NKCC1 or mGluR I inhibition on neuroprotection following OGD/REOX. A low level of cell death occurred in normoxic control neurons (13.8 ± 1.0 %). 2 h OGD and 22 h REOX triggered a significant increase in cell mortality (65.1 ± 2.8 %, $p < 0.05$, Figure 7 C). Inhibition of NKCC1 activity with 10 μM bumetanide either prior to OGD (32.7 ± 4.0 %, $p < 0.05$) or only during 0-24 h REOX (38.7 ± 4.2 %, $p < 0.05$) significantly attenuated OGD/REOX-mediated neuronal death. However, addition of bumetanide at 3 h REOX failed to reduce ischemic cell death.

Inhibition of mGluR I with 100 μM AIDA during 0-24 h REOX caused similar protection as bumetanide (43.3 ± 3.4 %, $p < 0.05$, Figure 7 D). Compared to bumetanide treatment alone, no additive effects were found in neuroprotection when either AIDA or 10 μM (-)-MK-801 was added together with bumetanide during 0-24 h REOX (Figure 7 D). These findings suggest that NKCC1 activity is important for neuronal damage during early REOX.

**Thermodynamic analysis of $NCX_{rev}$—**To further support the role of $NCX_{rev}$ in $Ca^{2+}$ homeostasis, we performed theoretical thermodynamic analysis of $NCX_{rev}$ in neurons with LabHEART [version 4.9.5 simulation software; (Puglisi and Bers 2001)]. The key variables, $[Na^+]_o$, $[Ca^{2+}]_o$, $[Na^+]_{cyt}$, and $[Ca^{2+}]_{cyt}$, were modified with our experimental data under normoxic control and 60 min REOX. The membrane voltage at which each simulation generated zero current was then plotted against $[Na^+]_{cyt}$ (Figure 8 A). Under control conditions, with a $[Ca^{2+}]_{cyt}$ of 68 nM, and $[Na^+]_{cyt}$ of 10 mM in neurons, the model predicts a reversal potential of −50 mV. At ~ 60 mV resting plasma membrane potential in cultured cortical neuron (Zhu et al. 2005), the forward-mode of NCX would be favored. At 60 min REOX, $[Ca^{2+}]_{cyt}$ rises to 334 nM. Although this increase in $[Ca^{2+}]_{cyt}$ would further favor the forward-mode operation of NCX, the significant concurrent increase in $[Na^+]_{cyt}$ strongly favors an inwardly directed $Ca^{2+}$ current via $NCX_{rev}$ (Figure 8 A). The simulation predicts that even if plasma membrane potential remains at −60 mV, NCX will function in the reverse mode when $[Na^+]_{cyt}$ increases to ~ 19 mM with $[Ca^{2+}]_{cyt}$ of 334 nM.

We also directly determined $NCX_{rev}$ in neurons at 0, 10 and 45 min REOX following 2 h OGD (Figure 8 B). When $NCX_{rev}$ was initiated in a $Na^+$-free/low $Ca^{2+}$ buffer, $Ca^{2+}$ influx rate was ~ 50 nM/min. In the presence of SEA0400 (1 μM), $NCX_{rev}$ was reduced by 90 % (Figure 8 B). Following 2 h OGD, $NCX_{rev}$ activity was increased by ~ 40%. 10 min REOX led to ~ 80% increase in $NCX_{rev}$ activity, which was doubled at 45 min REOX. This activation of $NCX_{rev}$ during post-OGD was nearly abolished with the $NCX_{rev}$ inhibitor SEA0400 (Figure 8 B). These data are consistent with the temporal changes of $[Na^+]_{cyt}$ as described above. Taken together, the role of $NCX_{rev}$ in $Ca^{2+}$ homeostasis following *in vitro* ischemia is supported by these studies.

## DISCUSSION

### Dysregulation of $Ca^{2+}_{ER}$ in cortical neurons following OGD/REOX

The disruption of $Ca^{2+}_{ER}$ homeostasis has been linked to numerous pathological conditions including neuronal death (Glazner and Fernyhough 2002). Depletion of $Ca^{2+}_{ER}$ has been suggested as an initial signal for ER dysfunction in ischemic neurons, based on high $IP_3R$ density and low SERCA in the vulnerable regions of the hippocampus, and expression of ER-resident stress proteins similar to that seen following thapsigargin-induced $Ca^{2+}_{ER}$ depletion (Paschen and Doutheil 1999). However, kinetic changes of $Ca^{2+}_{ER}$ during ischemia and post-ischemia are not well understood.

In the current study, we observed that 2 h OGD led to ~2 fold increase in thapsigargin-induced $Ca^{2+}$ release, which implies that OGD causes an increase in $Ca^{2+}_{ER}$ loading in neurons. Direct measurement of $Ca^{2+}_{ER}$ by the ER $Ca^{2+}$ fluorescence dye mag-fura 2 revealed an ~ 3 fold increase in $Ca^{2+}_{ER}$ at the end of 2 h OGD. The results from the two different methods are consistent and in agreement with the well defined function of ER in buffering of $Ca^{2+}_{cyt}$. Simulations from a quantitative model predict that mild depolarization in bullfrog sympathetic neurons would result in $Ca^{2+}_{cyt}$ elevation to 300-400 nM and an increase in $Ca^{2+}_{ER}$ (Albrecht et al. 2002). Our finding directly demonstrates that accumulation of $Ca^{2+}_{ER}$ occurs when the $Ca^{2+}_{cyt}$ level is moderately elevated during OGD.

Many studies with indirect measurement of $Ca^{2+}_{ER}$ reveal that there is a release of $Ca^{2+}_{ER}$ in ischemic neurons. When $Ca^{2+}_{ER}$ is depleted with cyclopiazonic acid or $Ca^{2+}_{ER}$ release is blocked by ryanodine receptor inhibition prior to OGD, aspiny interneurons show less increase in $Ca^{2+}_{cyt}$ (Pisani et al. 2000). These data suggest that a portion of the increase in $Ca^{2+}_{cyt}$ originates from ER under severe metabolic stress conditions.

In the current study, significant elevation of $IP_3$ content was detected in neurons during 5-10 min REOX. 85% loss of $Ca^{2+}_{ER}$ occurred within 15 min REOX. Inhibition of the $IP_3R$ with either 2-APB or xestospongin C blocked the $Ca^{2+}_{ER}$ release. This implies that $Ca^{2+}_{ER}$ release is largely mediated by $IP_3R$ activation during early REOX. Because activation of group I mGluR coupled with PLC can stimulate $IP_3$ production and release of $Ca^{2+}$ from ER (Bruno et al. 2001), we investigated whether inhibition of group I mGluR affected $Ca^{2+}_{ER}$ release. Indeed, group I mGluR antagonist AIDA nearly blocked OGD/REOX-mediated $Ca^{2+}_{ER}$ release. Moreover, we found that treatment of neurons with AIDA during 0-24 h REOX caused significant neuroprotection. Neuroprotective effects of inhibition of group I mGluRs have been shown in numerous reports (Bruno et al. 2001; Allen et al. 2000). Our study further suggests that group I mGluRs may be involved in ischemic damage in part via triggering $IP_3R$-mediated $Ca^{2+}_{ER}$ release and ER dysfunction (Figure 9).

## Role of NKCC1/$NCX_{rev}$ in disruption of $Ca^{2+}_{ER}$ following OGD/REOX

$NCX_{rev}$-mediated intracellular $Ca^{2+}$ overload following $[Na^+]_{cyt}$ elevation has been suggested as a contributing mechanism leading to neuronal death (Hoyt et al. 1998), axonal damage (Li et al. 2000), and astrocyte dysfunction (Kintner et al. 2006). On the other hand, it has been proposed that NCX operates in the forward mode to clear $Ca^{2+}$ in astrocytes from neonatal rat optic nerve during OGD/REOX (Fern 1998). In this study, we found that inhibition of NKCC1 during OGD prevented $Ca^{2+}_{ER}$ accumulation. This is because NKCC1-mediated $Na^+$ flux may trigger $Ca^{2+}$ influx through $NCX_{rev}$ and contribute to $Ca^{2+}_{ER}$ loading (Figure 9). This possibility has been confirmed with thermodynamic modeling analysis and $NCX_{rev}$ measurement (Figure 8). Our current findings suggest that coupling of NKCC1/$NCX_{rev}$ may play a role in $Ca^{2+}_{ER}$ release during REOX (Figure 9). We found that either application of bumetanide at 0 min REOX or genetic ablation of NKCC1 abolished the release of $Ca^{2+}_{ER}$. The role of $NCX_{rev}$ is further supported by our data with the $NCX_{rev}$ inhibitor SEA0400.

It has been reported that a significant portion of ischemic axoplasmic $Ca^{2+}$ increase originates from the ER and the $Ca^{2+}$ release is strongly dependent on axonal $Na^+$ influx (Nikolaeva et al. 2005). The authors speculate that ischemic $Na^+$ influx promotes glutamate release, which in turn stimulates mGluRs, activates PLC, and generates $IP_3$ (Nikolaeva et al. 2005). Although our data are consistent with the report on the dependency of $Ca^{2+}_{ER}$ release on accumulation of $Na^+_{cyt}$ and activation of $IP_3R$, the exact underlying cellular mechanisms which involve NKCC1/$NCX_{rev}$ remain to be determined. We speculate that inhibition of NKCC1/$NCX_{rev}$ reduces $Na^+_{cyt}$, $Ca^{2+}_{cyt,}$ and swelling (Figure 9). Presumably, these changes will attenuate glutamate release from both vesicle-mediated ($Ca^{2+}$-dependent) and swelling-induced (volume-sensitive organic anion channels) pathways. Therefore, when NKCC1 activity is inhibited by bumetanide, a reduced release of glutamate would lessen activation of mGluRs and subsequent $IP_3$ formation following ischemia. This view is supported by our $IP_3$ data. Moreover, inhibition of NKCC1 activity either pharmacologically or by genetic ablation significantly attenuates swelling of astrocytes and neurons as well as glutamate release from astrocytes (Su et al. 2002; Beck et al. 2003).

It has been suggested that $IP_3R$-mediated $Ca^{2+}_{ER}$ release can enter the adjacent mitochondria and trigger Cyt. C release (Rizzuto and Pozzan 2006). Cyt. C binds to $IP_3R$ and further augment $Ca^{2+}_{ER}$ release by inhibiting $Ca^{2+}$-mediated inhibition of $IP_3R$ (Hara and Snyder 2007). This feed-forward cycle of $Ca^{2+}$ transmission can cause synchronized $Ca^{2+}_{ER}$ release and apoptosis (Hara and Snyder 2007). We detected Cyt. C release at 1 h REOX following OGD and inhibition of NKCC1 with bumetanide not only blocked the $Ca^{2+}_{ER}$ release but also attenuated Cyt. C release and neuronal death. However, we did not monitor the time-dependent release of Cyt. C during the entire REOX period. It remains to be determined whether the feed-forward cycle plays a role in $Ca^{2+}_{ER}$ release following OGD/REOX.

### ER stress following OGD/REOX

Depletion of $Ca^{2+}_{ER}$ stores with thapsigargin can lead to ER stress (Paschen and Doutheil 1999), which induces suppression of protein synthesis, polyribosomal disaggregation, and activation of ER stress genes in neurons (Doutheil et al. 1997; Mengesdorf et al. 2001). This ER stress response is almost identical to the responses found in transient cerebral ischemia (Paschen et al. 1996). GRP78 is detached from PERK by 1-4 hour reperfusion following 30-min focal ischemia, which is accompanied by a significant increase in p-eIF2α (Hayashi et al. 2004). After 6 h reperfusion, the level of p-eIF2α is three fold higher than basal levels (Althausen et al. 2001). PERK is also activated by 10-min reperfusion following 10-min global ischemia (Kumar et al. 2003). PERK is the only kinase to phosphorylate eIF2α in ischemic brain at least during the early stage of reperfusion (DeGracia et al. 1999; Kumar et al. 2001). However, it is unknown whether this is the case in primary neurons after OGD/REOX.

In the current study, p-eIF2α signals were not changed during 2 h OGD but dramatically increased upon REOX. The p-eIF2α signals reached a peak level at 0.25 h REOX and remained elevated until 24 h REOX, which is different from *in vivo* ischemia (Althausen et al. 2001). This sustained elevation in p-eIF2α in neurons suggests that some type of stress, which is independent of intracellular ATP level, may be involved. We have reported that ATP is reduced by ~ 85% at 2 h OGD (Luo et al. 2005) and returned to ~ 50 % of control by 1 h REOX (data not shown). These changes in ATP levels are similar in differentiated PC12 cells, however, 4 h OGD in PC12 cells leads to a transient increase in p-eIF2α that then returns to the basal level by 30 min REOX (Munoz et al. 2000). This suggests that primary cortical neurons have less tolerance to ischemic insult and exhibit sustained UPR following OGD.

We observed that 2 h OGD led to 80% activation of caspase 12, which remained elevated during 15-60 min REOX. GRP78 protein elevation and caspase 12 activation occurred at 2 h OGD when $Ca^{2+}_{ER}$ was significantly loaded. The increase of p-eIF2a level did not occur until $Ca^{2+}_{ER}$ was depleted during REOX. These data imply that altered $Ca^{2+}_{ER}$ homeostasis (either overload or depletion) may trigger ER dysfunction and ER stress.

Inhibition of NKCC1 activity with its inhibitor bumetanide during OGD and REOX significantly reduced the up-regulation of GRP78, expression of p-eIF2α, and activation of caspase 12 during REOX. Similar results of p-eIF2α were found in $NKCC1^{-/-}$ neurons. These data suggest that NKCC1 activation is involved in ER stress development. Bumetanide pretreatment-mediated effects on ER stress may result from less $Ca^{2+}_{ER}$ loading during OGD and subsequent less release of $Ca^{2+}_{ER}$ during REOX. Moreover, inhibition of NKCC1 during REOX also shows some protective effects. This may result from less glutamate release and retention of $Ca^{2+}_{ER}$ as discussed above.

In the case of GRP78, 2 h OGD induced 50 % up-regulation of GRP78 protein, which remained elevated during 1-12 h REOX. Multiple mechanisms, including glucose deprivation, govern GRP78 expression (Shiu et al. 1977; Shintani-Ishida et al. 2006). The OGD-mediated upregulation of GRP78 may in part result from both glucose deprivation and changes of $Ca^{2+}_{ER}$. Moreover, the high p-eIF2α levels during REOX may inhibit protein synthesis and could preclude further increases in GRP78 expression.

In summary, we report here that biphasic changes in $Ca^{2+}_{ER}$ were triggered in neurons following OGD and REOX. NKCC1 and $NCX_{rev}$ are involved in the overload of $Ca^{2+}_{ER}$ during OGD and $IP_3R$-mediated release of $Ca^{2+}_{ER}$ during REOX. The changes of $Ca^{2+}_{ER}$ were concurrently accompanied with elevation of several ER stress markers such as p-eIF2α, caspase 12 cleavage, and GRP78. Reduction of $Ca^{2+}_{ER}$ disruption by blocking of NKCC1/$NCX_{rev}$ significantly attenuated ER stress proteins and cell death.

## The abbreviations used

| | |
|---|---|
| Cyt. C | cytochrome C |
| eIF2α | eukaryotic initiation factor 2α |
| ER | endoplasmic reticulum |
| GRP78 | glucose regulated protein 78 |
| ICS | intracellular solution |
| $IP_3$ | inositol 1,4,5-trisphosphate |
| $IP_3R$ | inositol 1,4,5-trisphosphate receptor |
| mGluR I | group I metabotropic glutamate receptor |
| NCX | $Na^+/Ca^{2+}$ exchanger |
| $NCX_{rev}$ | reversed mode operation of NCX |
| NKCC1 | $Na^+$-$K^+$-$Cl^-$ cotransporter isoform 1 |
| OGD | Oxygen and glucose deprivation |
| PERK | RNA-dependent protein kinase-like ER kinase |
| PLC | phospholipase C |
| REOX | reoxygenation |
| SERCA | sarco/endoplasmic reticulum $Ca^{2+}$-ATPase |
| UPR | unfolded protein response |

## REFERENCES


Albrecht MA, Colegrove SL, Friel DD. Differential regulation of ER $Ca^{2+}$ uptake and release rates accounts for multiple modes of $Ca^{2+}$-induced $Ca^{2+}$ release. J Gen Physiol 2002;119:211–233. [PubMed: 11865019]

Allen JW, Knoblach SM, Faden AI. Activation of group I metabotropic glutamate receptors reduces neuronal apoptosis but increases necrotic cell death in vitro. Cell Death Differ 2000;7:470–476. [PubMed: 10800080]

Althausen S, Mengesdorf T, Mies G, Olah L, Nairn AC, Proud CG, Paschen W. Changes in the phosphorylation of initiation factor eIF-2 alpha, elongation factor eEF-2 and p70 S6 kinase after transient focal cerebral ischaemia in mice. J Neurochem 2001;78:779–787. [PubMed: 11520898]

Beck J, Lenart B, Kintner DB, Sun D. Na-K-Cl cotransporter contributes to glutamate-mediated excitotoxicity. J Neurosci 2003;23:5061–5068. [PubMed: 12832529]

Bruno V, Battaglia G, Copani A, D'Onofrio M, Di Iorio P, De Blasi A, Melchiorri D, Flor PJ, Nicoletti F. Metabotropic glutamate receptor subtypes as targets for neuroprotective drugs. J Cereb Blood Flow Metab 2001;21:1013–1033. [PubMed: 11524608]

Chen H, Luo J, Kintner DB, Shull GE, Sun D. $Na^+$-dependent chloride transporter (NKCC1)-null mice exhibit less gray and white matter damage after focal cerebral ischemia. J Cereb Blood Flow Metab 2005;25:54–66. [PubMed: 15678112]

Corbett EF, Michalak M. Calcium, a signaling molecule in the endoplasmic reticulum? Trends Biochem Sci 2000;25:307–311. [PubMed: 10871879]

DeGracia DJ, Adamczyk S, Folbe AJ, Konkoly LL, Pittman JE, Neumar RW, Sullivan JM, Scheuner D, Kaufman RJ, White BC, Krause GS. Eukaryotic initiation factor 2 alpha kinase and phosphatase activity during postischemic brain reperfusion. Exp Neurol 1999;155:221–227. [PubMed: 10072297]

DeGracia DJ, Hu BR. Irreversible translation arrest in the reperfused brain. J Cereb Blood Flow Metab 2007;27:875–893. [PubMed: 16926841]

DeGracia DJ, Montie HL. Cerebral ischemia and the unfolded protein response. J Neurochem 2004;91:1–8. [PubMed: 15379881]

Doutheil J, Gissel C, Oschlies U, Hossmann KA, Paschen W. Relation of neuronal endoplasmic reticulum calcium homeostasis to ribosomal aggregation and protein synthesis: implications for stress-induced suppression of protein synthesis. Brain Res 1997;775:43–51. [PubMed: 9439827]

Fern R. Intracellular calcium and cell death during ischemia in neonatal rat white matter astrocytes in situ. J Neurosci 1998;18:7232–7243. [PubMed: 9736645]

Flagella M, Clarke LL, Miller ML, Erway LC, Giannella RA, Andringa A, Gawenis LR, Kramer J, Duffy JJ, Doetschman T, Lorenz JN, Yamoah EN, Cardell EL, Shull GE. Mice lacking the basolateral Na-K-2Cl cotransporter have impaired epithelial chloride secretion and are profoundly deaf. J Biol Chem 1999;274:26946–26955. [PubMed: 10480906]

Glazner GW, Fernyhough P. Neuronal survival in the balance: are endoplasmic reticulum membrane proteins the fulcrum? Cell Calcium 2002;32:421–433. [PubMed: 12543101]

Groenendyk J, Michalak M. Endoplasmic reticulum quality control and apoptosis. Acta Biochim Pol 2005;52:381–395. [PubMed: 15933766]

Grynkiewicz G, Poenie M, Tsien RY. A new generation of $Ca^{2+}$ indicators with greatly improved fluorescence properties. J Biol Chem 1985;260:3440–3450. [PubMed: 3838314]

Hara MR, Snyder SH. Cell signaling and neuronal death. Annu Rev Pharmacol Toxicol 2007;47:117–141. [PubMed: 16879082]

Hayashi T, Saito A, Okuno S, Ferrand-Drake M, Dodd RL, Chan PH. Oxidative injury to the endoplasmic reticulum in mouse brains after transient focal ischemia. Neurobiol Dis 2004;15:229–239. [PubMed: 15006693]

Hayashi T, Saito A, Okuno S, Ferrand-Drake M, Dodd RL, Chan PH. Damage to the endoplasmic reticulum and activation of apoptotic machinery by oxidative stress in ischemic neurons. J Cereb Blood Flow Metab 2005;25:41–53. [PubMed: 15678111]

Hayashi T, Saito A, Okuno S, Ferrand-Drake M, Dodd RL, Nishi T, Maier CM, Kinouchi H, Chan PH. Oxidative damage to the endoplasmic reticulum is implicated in ischemic neuronal cell death. J Cereb Blood Flow Metab 2003;23:1117–1128. [PubMed: 14526222]

Hoyt KR, Arden SR, Aizenman E, Reynolds IJ. Reverse $Na^+/Ca^{2+}$ exchange contributes to glutamate-induced intracellular $Ca^{2+}$ concentration increases in cultured rat forebrain neurons. Mol Pharmacol 1998;53:742–749. [PubMed: 9547366]

Kintner DB, Luo J, Gerdts J, Ballard AJ, Shull GE, Sun D. $Na^+$-$K^+$-$Cl^-$ cotransport and $Na^+/Ca^{2+}$ exchange in astrocyte mitochondrial dysfunction in response to in vitro ischemia. J Neurosci. 2006

Kintner DB, Luo J, Gerdts J, Ballard AJ, Shull GE, Sun D. Role of $Na^+$-$K^+$-$Cl^-$ cotransport and $Na^+/Ca^{2+}$ exchange in mitochondrial dysfunction in astrocytes following in vitro ischemia. Am J Physiol Cell Physiol 2007;292:C1113–C1122. [PubMed: 17035299]

Kintner DB, Su G, Lenart B, Ballard AJ, Meyer JW, Ng LL, Shull GE, Sun D. Increased tolerance to oxygen and glucose deprivation in astrocytes from $Na^+/H^+$ exchanger isoform 1 null mice. Am J Physiol Cell Physiol 2004;287:C12–C21. [PubMed: 15013953]

Kumar R, Azam S, Sullivan JM, Owen C, Cavener DR, Zhang P, Ron D, Harding HP, Chen JJ, Han A, White BC, Krause GS, DeGracia DJ. Brain ischemia and reperfusion activates the eukaryotic initiation factor 2 alpha kinase, PERK. J Neurochem 2001;77:1418–1421. [PubMed: 11389192]

Kumar R, Krause GS, Yoshida H, Mori K, DeGracia DJ. Dysfunction of the unfolded protein response during global brain ischemia and reperfusion. J Cereb Blood Flow Metab 2003;23:462–471. [PubMed: 12679723]

Lenart B, Kintner DB, Shull GE, Sun D. Na-K-Cl cotransporter-mediated intracellular $Na^+$ accumulation affects $Ca^{2+}$ signaling in astrocytes in an in vitro ischemic model. J Neurosci 2004;24:9585–9597. [PubMed: 15509746]

Li S, Jiang Q, Stys PK. Important role of reverse $Na^+$-$Ca^{2+}$ exchange in spinal cord white matter injury at physiological temperature. J Neurophysiol 2000;84:1116–1119. [PubMed: 10938336]

Luo J, Chen H, Kintner DB, Shull GE, Sun D. Decreased neuronal death in $Na^+/H^+$ exchanger isoform 1-null mice after in vitro and in vivo ischemia. J Neurosci 2005;25:11256–11268. [PubMed: 16339021]

Mengesdorf T, Althausen S, Oberndorfer I, Paschen W. Response of neurons to an irreversible inhibition of endoplasmic reticulum $Ca^{2+}$-ATPase: relationship between global protein synthesis and expression and translation of individual genes. Biochem J 2001;356:805–812. [PubMed: 11389688]

Munoz F, Martin ME, Manso-Tomico J, Berlanga J, Salinas M, Fando JL. Ischemia-induced phosphorylation of initiation factor 2 in differentiated PC12 cells: role for initiation factor 2 phosphatase. J Neurochem 2000;75:2335–2345. [PubMed: 11080185]

Nikolaeva MA, Mukherjee B, Stys PK. $Na^{+}$-dependent sources of intra-axonal $Ca^{2+}$ release in rat optic nerve during in vitro chemical ischemia. J Neurosci 2005;25:9960–9967. [PubMed: 16251444]

Paschen W. Endoplasmic reticulum: a primary target in various acute disorders and degenerative diseases of the brain. Cell Calcium 2003;34:365–383. [PubMed: 12909082]

Paschen W, Doutheil J. Disturbances of the functioning of endoplasmic reticulum: a key mechanism underlying neuronal cell injury? J Cereb Blood Flow Metab 1999;19:1–18. [PubMed: 9886350]

Paschen W, Doutheil J, Gissel C, Treiman M. Depletion of neuronal endoplasmic reticulum calcium stores by thapsigargin: effect on protein synthesis. J Neurochem 1996;67:1735–1743. [PubMed: 8858960]

Petr MJ, Wurster RD. Determination of *in situ* dissociation constant for Fura-2 and quantitation of background fluorescence in astrocyte cell line U373-MG. Cell Calcium 1997;21:233–240. [PubMed: 9105732]

Pisani A, Bonsi P, Centonze D, Giacomini P, Calabresi P. Involvement of intracellular calcium stores during oxygen/glucose deprivation in striatal large aspiny interneurons. J Cereb Blood Flow Metab 2000;20:839–846. [PubMed: 10826535]

Puglisi JL, Bers DM. LabHEART: an interactive computer model of rabbit ventricular myocyte ion channels and Ca transport. Am J Physiol Cell Physiol 2001;281:C2049–C2060. [PubMed: 11698264]

Rizzuto R, Pozzan T. Microdomains of intracellular $Ca^{2+}$: molecular determinants and functional consequences. Physiol Rev 2006;86:369–408. [PubMed: 16371601]

Russell JM. Sodium-potassium-chloride cotransport. Physiol Rev 2000;80:211–276. [PubMed: 10617769]

Shintani-Ishida K, Nakajima M, Uemura K, Yoshida K. Ischemic preconditioning protects cardiomyocytes against ischemic injury by inducing GRP78. Biochem Biophys Res Commun 2006;345:1600–1605. [PubMed: 16735028]

Shiu RP, Pouyssegur J, Pastan I. Glucose depletion accounts for the induction of two transformation-sensitive membrane proteinsin Rous sarcoma virus-transformed chick embryo fibroblasts. Proc Natl Acad Sci U S A 1977;74:3840–3844. [PubMed: 198809]

Su G, Kintner DB, Flagella M, Shull GE, Sun D. Astrocytes from $Na^{+}$-$K^{+}$-$Cl^{-}$ cotransporter-null mice exhibit absence of swelling and decrease in EAA release. Am J Physiol Cell Physiol 2002;282:C1147–C1160. [PubMed: 11940530]

Tsien, RW.; Pozzan, T. Measurement of Cytosolic Free $Ca^{2+}$ with Quin2. In: Fleischer, S., editor. Biomembranes. Part S, Transport : membrane isolation and characterization. Academic Press; San Diego: 1989. p. 230-262.

Urbanczyk J, Chernysh O, Condrescu M, Reeves JP. Sodium-calcium exchange does not require allosteric calcium activation at high cytosolic sodium concentrations. J Physiol 2006;575:693–705. [PubMed: 16809364]

Zhu L, Lovinger D, Delpire E. Cortical neurons lacking $KCC_2$ expression show impaired regulation of intracellular chloride. J Neurophysiol 2005;93:1557–1568. [PubMed: 15469961]

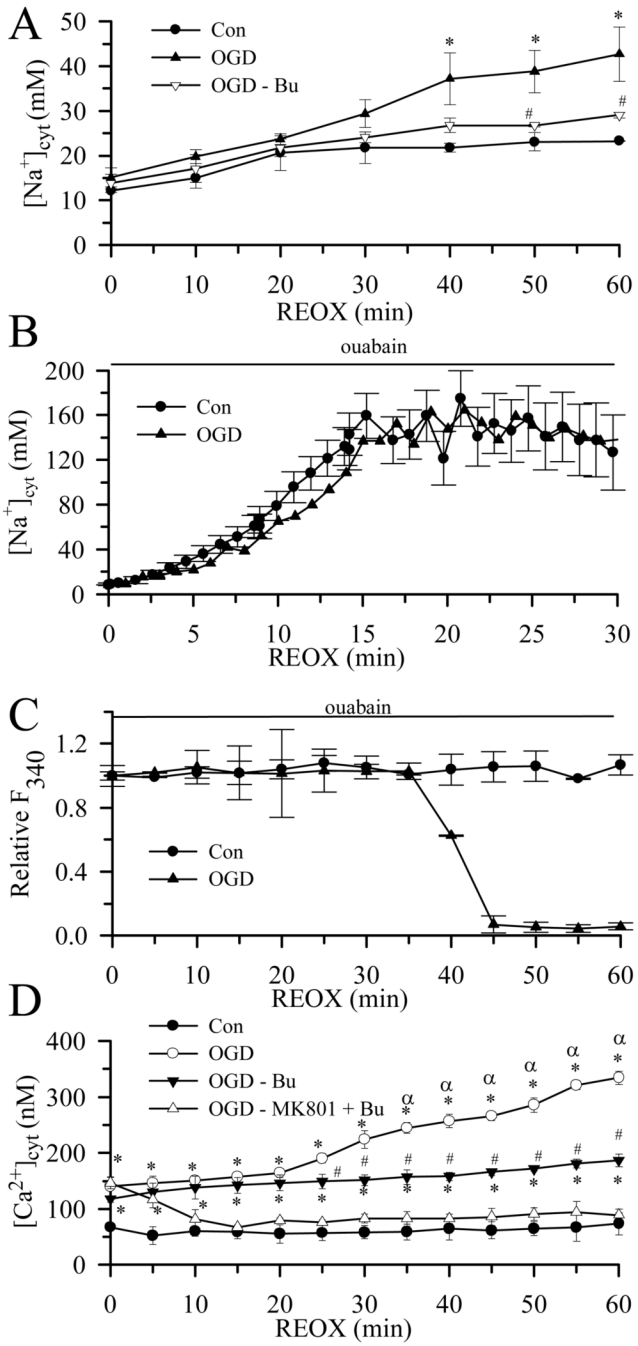


**Figure 1. Changes of $[Na^+]_{cyt}$ and $[Ca^{2+}]_{cyt}$ in neurons during REOX**

$[Na^+]_{cyt}$ **(A, B)** and $[Ca^{2+}]_{cyt}$ **(D)** were monitored during 30-60 min REOX in single neurons following 2 h OGD. In studies with bumetanide, bumetanide (5 μM) was present during both OGD and REOX. In the double treatment study, (−)-MK-801 (10 μM) and bumetanide (5 μM) were added at 0 min REOX. Data are means ± SEM, n=3-4. Means were compared using a One-Way ANOVA with a Bonferroni post-hoc test. * $p < 0.05$ vs. Con; # $p < 0.05$ vs. non-treated OGD; α < 0.05 vs. 0 min REOX. In **B,** in ouabain (1 mM)-treated neurons, the data are expressed as means ± SD of 15-20 cells for each condition. **(C)** Ouabain-induced changes of relative SBFI fluorescence at 340 nm are shown. The sudden loss of fluorescence represents

loss of plasma membrane integrity and cell death. Data are means ± SD of 2-3 cells for each condition.

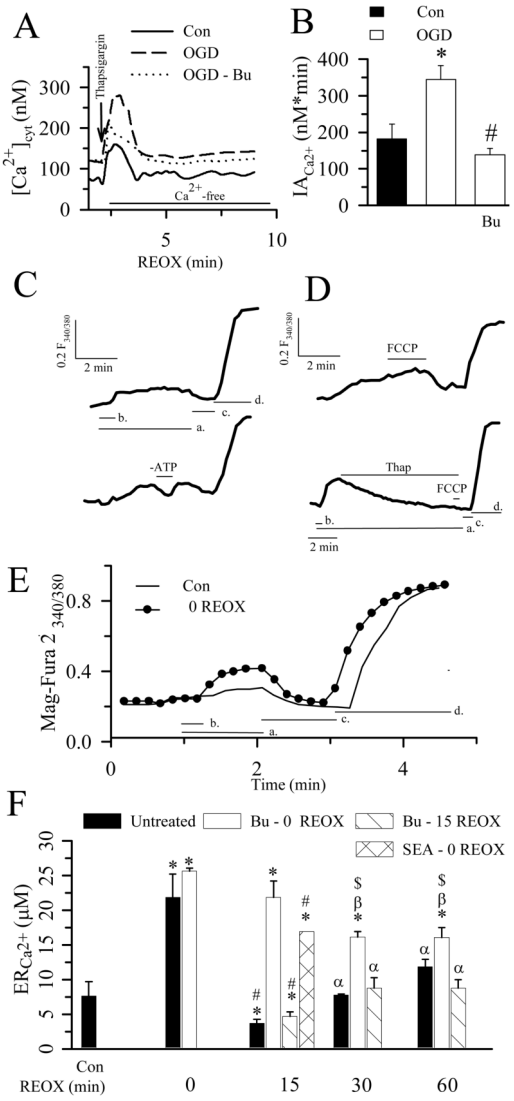


**Figure 2. Changes of $Ca^{2+}_{ER}$ in neurons during REOX**

**A.** Thapsigargin-mediated release of $Ca^{2+}_{ER}$ in single neurons was determined with fura-2 during 2-5 min REOX following 2 h OGD. Thapsigargin (1 μM) was applied under $[Ca^{2+}]_o$-free conditions. Bumetanide (Bu, 5 μM) was present during both OGD and REOX. **B.** Summary data. Data are means ± SEM. n = 3-4. Means were compared using a student's *t*-test. * $p < 0.05$ vs. Con; # $p < 0.05$ vs. OGD. **C.** Representative traces for $Ca^{2+}_{ER}$ determination by measuring 340 nm/380 nm fluorescence of mag-fura 2. In the top trace, cells were in a solution mimicking intracellular ion concentrations **(a)** and permeablized by a brief exposure to saponin (**b**). The post-saponin 340/380 fluorescence ($Ca^{2+}_{ER}$) was calibrated by exposing cells to zero $Ca^{2+}$ ($R_{min}$, **c**) and 10 mM $Ca^{2+}$ containing solutions ($R_{max}$, **d**). In the bottom trace, ATP was removed (-ATP) from the solution to confirm the ATP dependency of the mag-fura 2 fluorescence. Tracings are identically scaled, but off-set to provide clarity. **D.** Response of mag-fura 2 signals to 1 μM FCCP (top trace) or to 1 μM thapsigargin followed by 1 μM FCCP (bottom trace). Note that the time scale in the bottom trace is somewhat longer than the upper trace. This is due to the slower response of $Ca^{2+}_{ER}$ to thapsigargin compared to FCCP. **E.** Changes of mag-fura 2 signals in normoxic control or 2 h OGD-treated neurons. **F.** Summary data of $Ca^{2+}_{ER}$ at 2 h OGD and 0, 15, 30, or 60 min REOX. In bumetanide experiments, the

drug was applied at 0 or 15 REOX. The $NCX_{rev}$ antagonist SEA0400 (1 μM) was applied at 0 REOX. Data are means ± SEM. n = 4-6. Means were compared using a One-Way ANOVA with a Bonferroni post-hoc test. * $p < 0.05$ vs. Con; $^{\#}$ $p < 0.05$ vs. 0 min REOX; α $p < 0.05$ vs. 15 min REOX; β $p < 0.05$ vs. 0 min Bu-REOX; $ $p < 0.05$ vs. untreated group.

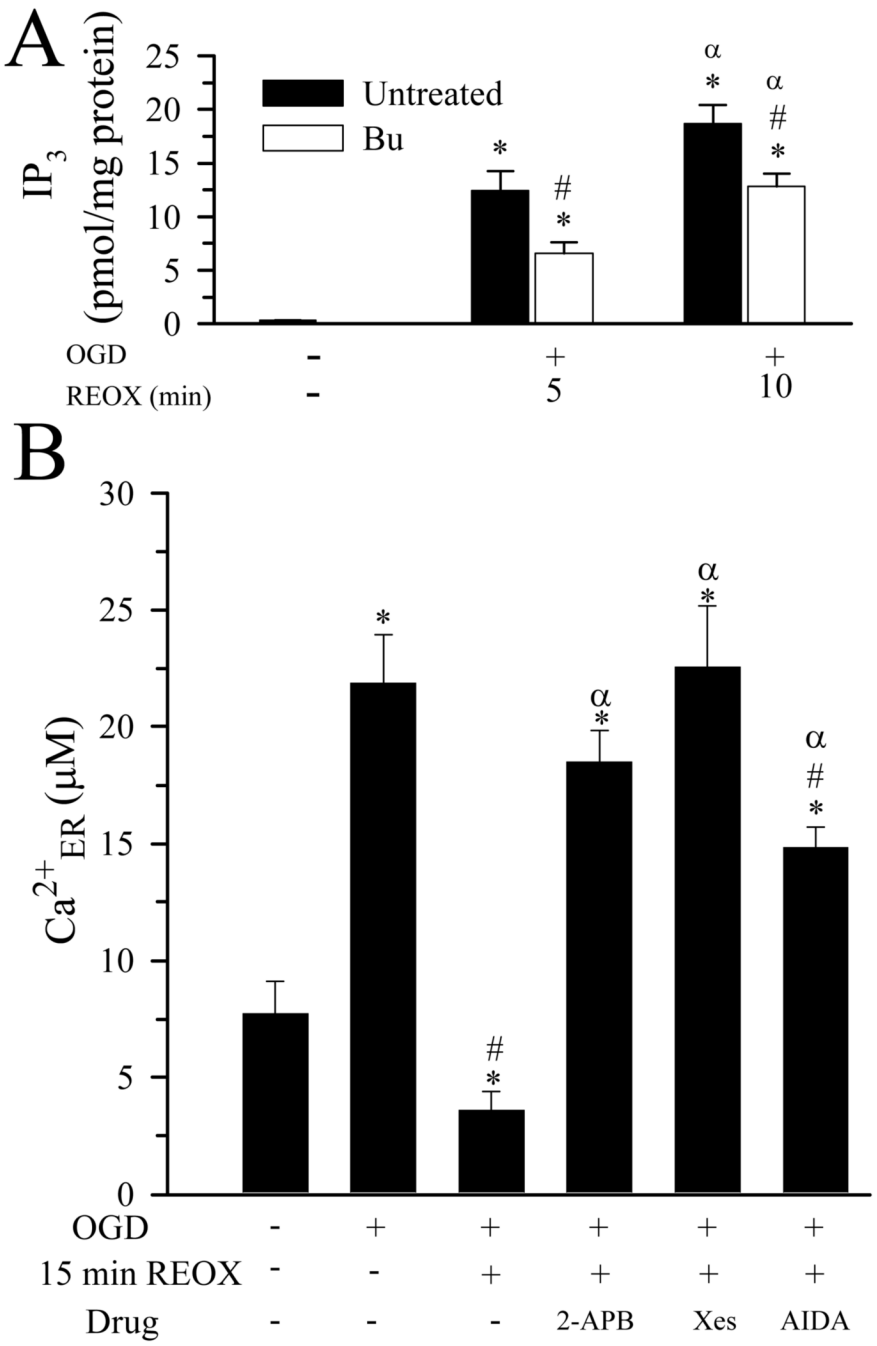


**Figure 3. $IP_3$ formation and its role in OGD/REOX-induced $Ca^{2+}_{ER}$ release**

**A.** $IP_3$ levels in pure neuronal cultures were determined under basal conditions and at 5 or 10 min REOX. In bumetanide experiments, bumetanide was present during OGD and REOX. Data are means ± SEM. n = 3. Means were compared with a student's *t*-test. * $p < 0.05$ vs. Con; # $p < 0.05$ vs. untreated; α $p < 0.05$ vs. 10 min REOX. **B.** $IP_3$ receptor antagonists 2-APB (100 μM) or xestospongin C (20 μM) or the mGluR I antagonist AIDA (100 μM) were applied at the end of OGD. $Ca^{2+}_{ER}$ was determined at 15 min of REOX. Data are means ± SEM. n = 3-4. Means were compared using a One-Way ANOVA with a Bonferroni post-hoc test. * $p < 0.05$ vs. Con; # $p < 0.05$ vs. 0 min REOX; α $p < 0.05$ vs. 15 min REOX.

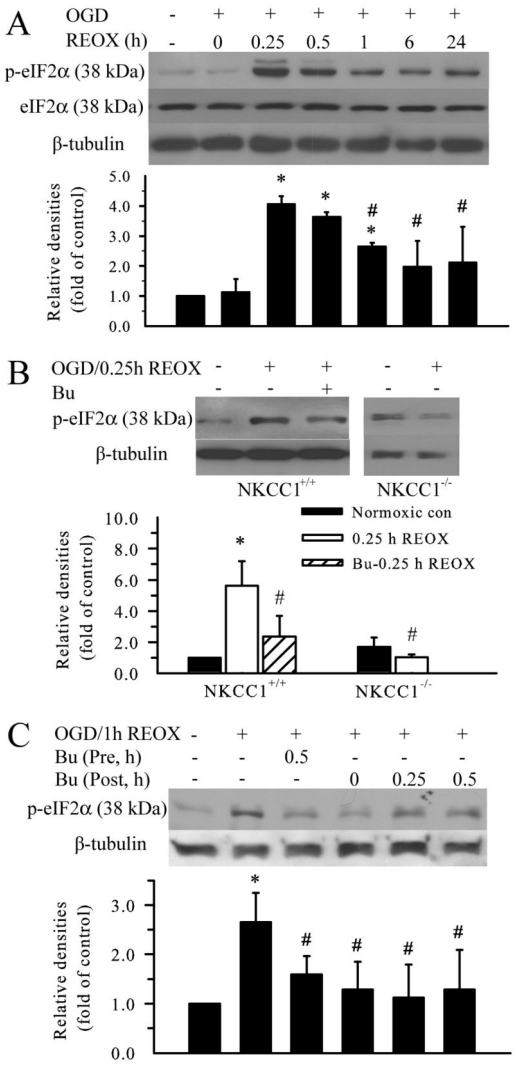


**Figure 4. Inhibition of NKCC1 activity attenuates OGD/REOX-mediated upregulation of p-eIF2α**

**A**. Expression of p-eIF2α protein was determined at 2 h OGD, or 0.25, 0.5, 1, 6, and 24 h REOX. Levels of total eIF2α and β tubulin were shown for loading controls. The bar graph represents the relative expression of p-eIF2α protein estimated from the mean pixel density normalized to β tubulin. **B.** Effect of NKCC1 inhibitor bumetanide or gene ablation of NKCC1 on p-eIF2α protein expression. $NKCC1^{+/+}$ neurons were treated with 10 μM bumetanide 30 min prior to OGD and the drug was present in all subsequent incubations. In gene ablation studies, $NKCC1^{+/+}$ or $NKCC1^{-/-}$ neuronal cultures were prepared from $NKCC1^{+/+}$ and $NKCC1^{-/-}$ littermates. The mean data of the $NKCC1^{+/+}$ cultures were then pooled together with the original data sets, so systematic differences were reduced to the minimum. Data in A-B are means ± SD. n = 3. * $p < 0.05$ vs. $NKCC1^{+/+}$ con; # $p < 0.05$ vs. $NKCC1^{+/+}$ 0.25 h REOX. **C**. Bumetanide post-ischemia treatment. 10 μM bumetanide was applied at 0, 0.25 or 0.5 h REOX. Expression of p-eIF2α protein was determined at 1 h REOX. Data are means ± SD. n = 3. Means were compared using a One-Way ANOVA with a Bonferroni post-hoc test. * $p < 0.05$ vs. con; # $p < 0.05$ vs. 1 h REOX.

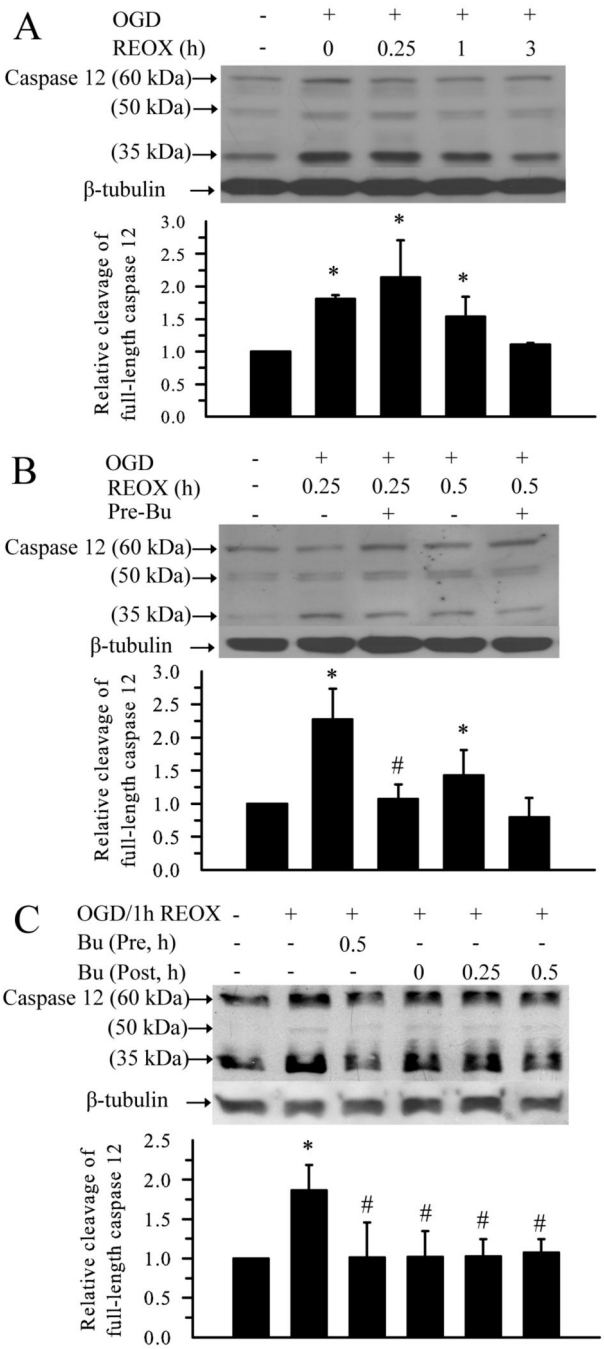


**Figure 5.**

Inhibition of NKCC1 activity reduces OGD/REOX-mediated caspase 12 activation

**A.** Changes of caspase 12 protein at 2 h OGD and 0.25, 1, or 3 h REOX. Relative activation of caspase 12 was determined by the ratio of the cleavage bands (35 kDa + 50 kDa) vs. 60 kDa full length band. Sister cultures were incubated in normoxic buffers as control. **B.** Effect of bumetanide pre-ischemia treatment on the caspase 12 protein expression. Cells were pretreated with 10 μM bumetanide for 30 min and the drug was present in all subsequent incubations. Cells were then collected at either 0.25 h or 0.5 h REOX. Data are means ± SD. n = 3-4. Means were compared using a One-Way ANOVA with a Bonferroni post-hoc test. * $p < 0.05$ vs. Con; # $p < 0.05$ vs. 0.25 h REOX. **C.** Effect of bumetanide post-ischemia treatment on caspase

12 protein expression. 10 μM bumetanide was applied to cultures at 0, 0.25 or 0.5 h REOX. Cells were collected at 1 h REOX. Data are means ± SD. n = 3. * $p < 0.05$ vs. Con; $^{\#}$ $p < 0.05$ vs. 1 h REOX.

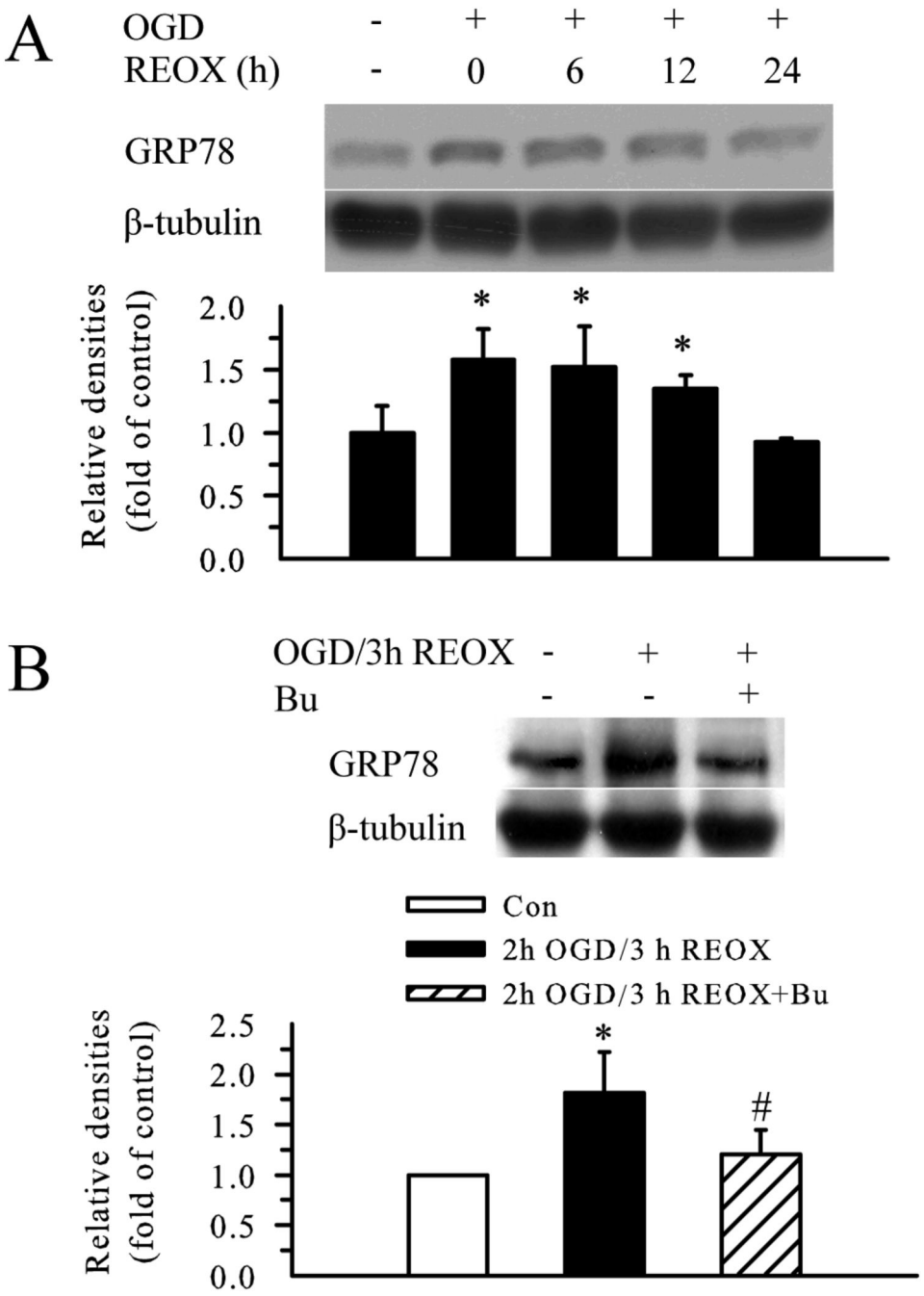


**Figure 6. Inhibition of NKCC1 activity reduces OGD/REOX-mediated GRP78 upregulation**

**A**. Expression of GRP78 protein at 2 h OGD or at 6, 12, and 24 h REOX. The bar graph represents the relative expression in GRP78 protein normalized to β tubulin. **B.** Effect of bumetanide pre-ischemia treatment on GRP78 protein expression. Data are means ± SD. n = 3. Means were compared using a One-Way ANOVA with a Bonferroni post-hoc test. * $p < 0.05$ vs. Con.; # $p < 0.05$ vs. REOX.

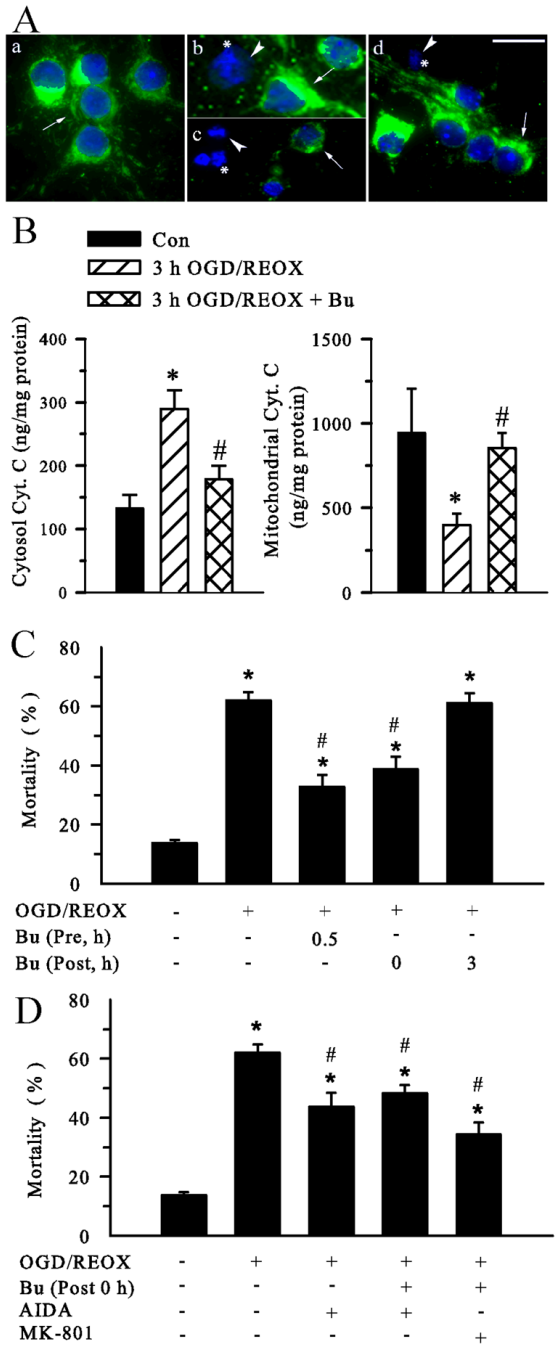


**Figure 7. Inhibition of NKCC1 activity reduces OGD/REOX-mediated Cyt. C release and neuronal death**

**A.** Cyt. C release in neurons was visualized by immunofluorescence staining. a - d: double staining with the Cyt. C antibody and DAPI. Images shown are representative of 4 experiments. For bumetanide treatment, neurons were incubated in EMEM in the presence of 10 μM Bu at 37°C during 3 h OGD and 21 h REOX. Sister cultures were incubated for 24 h in normoxic control buffers as controls (Con). **a.** Con. **b**. 3 h OGD/1 h REOX. **c.** 3 h OGD/21 h REOX. **d.** 3 h OGD/21 h REOX plus 10 μM Bu. Scale bar, 20 μm. **Arrow**: cells with retained Cyt. C; **Arrowhead:** loss of Cyt. C; *****: nuclei displayed with condensed or fragmented chromatin. **B.** Cyt. C content in cytosolic fraction (**left)** and mitochondrial fraction (**right)** was determined

in Con, 3 h OGD/21h REOX, or 3 h OGD/21h REOX plus Bu. Data are means ± SD. n = 3. Means were compared using a One-Way ANOVA with a Bonferroni post-hoc test. * $p < 0.05$ vs. Con; # $p < 0.05$ vs. OGD/REOX. **C.** Neuronal protection with bumetanide (10 μM) during OGD or REOX. Cell mortality was assessed after 2 h OGD and 22 h REOX. **D**. No additive effects with AIDA or (−)-MK-801. For drug treatment, neurons were incubated in EMEM containing 100 μM AIDA or 10 μM (−)-MK-801 during 0-22 h REOX. Data are means ± SEM. n = 4-8. * $p < 0.05$ vs. Con. # $p < 0.05$ vs. OGD/REOX.

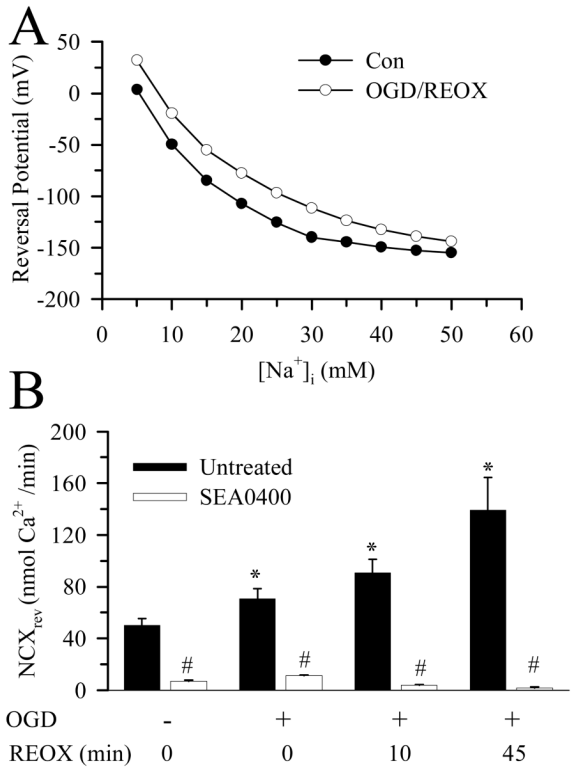


**Figure 8. $NCX_{rev}$ and its dependence on intracellular $Na^+$**

**A**. The NCX module of the LabHEART version 4.9.5 software was used to model changes in NCX reversal potential with intracellular $Na^+$ under control and OGD/REOX conditions. It is assumed that NCX is an electrogenic mechanism that transports $Na^+$ and $Ca^{2+}$ with a stoichiometry of 3:1. Values of $Na^+$ and $Ca^{2+}$ affinities, voltage saturation, and the position of the energy barrier were set at the default values for the simulator. I-V curves for NCX were generated with known values of extracellular $Na^+$ and $Ca^{2+}$ (**Methods**) and intracellular $Ca^{2+}$ and $Na^+$ values (Figure 1). For each intracellular $Na^+$ value, the reversal potential was taken as the voltage when NCX current equaled zero. **B.** $NCX_{rev}$ was determined under normoxic conditions and at 0, 10, and 60 min REOX following 2 h OGD. In SEA0400 experiments, SEA0400 (1 μM) was present throughout the $NCX_{rev}$ determination period. Data are the means ± SD of 15-20 cells from one coverslip for each condition. Means were compared using a One-Way ANOVA with a Bonferroni post-hoc test. * $p < 0.05$ vs. con, # $p < 0.05$ vs. non-treated.

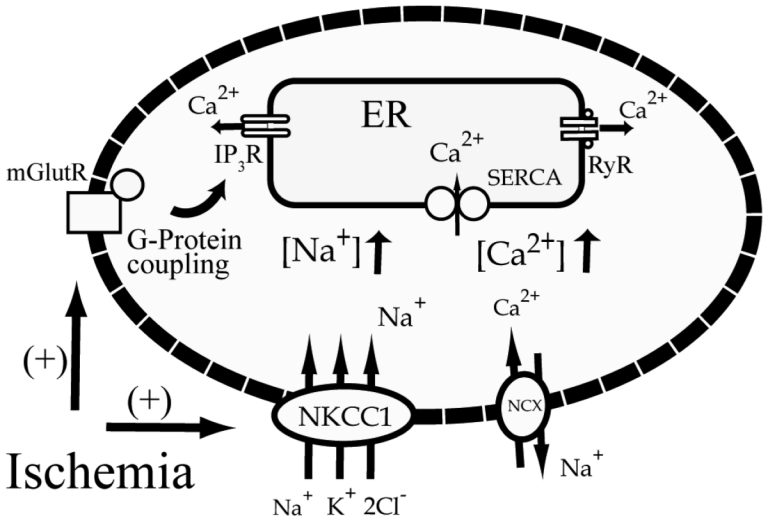


**Figure 9. A proposed mechanism for a role of NKCC1 and $NCX_{rev}$ in $Ca^{2+}_{ER}$ dysregulation following *in vitro* ischemia**

Following ischemia, activation of NKCC1 causes an increase in $[Na^+]_{cyt}$ which triggers $NCX_{rev}$ and leads to increases in $[Ca^{2+}]_{cyt}$. The $[Ca^{2+}]_{cyt}$ overload is initially buffered by SERCA and results in $Ca^{2+}_{ER}$ overload during ischemia. $Ca^{2+}_{ER}$ release subsequently occurs via activation of $IP_3R$ and mGluR-mediated pathways.